HHS Public Access

Author manuscript

Biomaterials. Author manuscript; available in PMC 2016 November 01.

Published in final edited form as:

Biomaterials. 2015 November ; 69: 184–190. doi:10.1016/j.biomaterials.2015.07.056.

Hydrophilic Packaging of Iron Oxide Nanoclusters for Highly Sensitive Imaging

Cartney E. Smith[a], **Dawn Ernenwein**[b], **Artem Shkumatov**[c,d], **Nicholas Clay**[a], **JuYeon Lee**[b], **Molly Melhem**[d,e], **Sanjay Misra**[f], **Steven C. Zimmerman**[b], and **Hyunjoon Kong**[a,d,*]

[a]Department of Chemical and Biomolecular Engineering, University of Illinois at Urbana-Champaign, 600 South Mathews Avenue, Urbana IL, 61801, USA

[b]Department of Chemistry, University of Illinois at Urbana-Champaign, 600 South Mathews Avenue, Urbana IL, 61801, USA

[c]Department of Pathobiology, College of Veterinary Medicine, University of Illinois at Urbana-Champaign, 2001 South Lincoln Avenue, Urbana, Illinois 61801, United States

[d]Institute for Genomic Biology, University of Illinois at Urbana-Champaign, 1206 West Gregory Drive, Urbana IL, 61801, USA

[e]Department of Bioengineering, University of Illinois at Urbana-Champaign, 1304 West Springfield Avenue, Urbana, Illinois 61801, United States

[f]Department of Radiology, Mayo Clinic, 200 First Street SW, Rochester MN, 55905, USA

Abstract

Superparamagnetic iron oxide nanoparticles (SPIONs) are used as imaging probes to provide contrast in magnetic resonance images. Successful use of SPIONs in targeted applications greatly depends on their ability to generate contrast, even at low levels of accumulation, in the tissue of interest. In the present study, we report that SPION nanoclusters packaged to a controlled size by a hyperbranched polyglycerol (HPG) can target tissue defects and have a high relaxivity of 719 $mM^{-1}s^{-1}$, which was close to their theoretical maximal limit. The resulting nanoclusters were able to identify regions of defective vasculature in an ischemic murine hindlimb using MRI with iron doses that were 5–10 fold lower than those typically used in preclinical studies. Such high relaxivity was attributed to the molecular architecture of HPG, which mimics that of the water retentive polysaccharide, glycogen. The results of this study will be broadly useful in sensitive imaging applications.

Keywords

nanocluster; molecular architecture; contrast agent; diagnostic imaging; polyglycerol

[*]**Corresponding Author**. hjkong06@illinois.edu, Fax: 217-333-5052.

1. Introduction

Magnetic resonance imaging (MRI) generates high-resolution images non-invasively and therefore is used for diagnosis of various tissue defects[1, 2] as well as evaluation of fluid flows within engineered materials and devices.[3–5] The diagnostic capability of MRI has been greatly enhanced with the introduction of superparamagnetic iron oxide nanoparticles (SPIONs), which can provide negative contrast against surrounding tissues. To further enhance their utility, SPIONs that have increased relaxivity while localizing at sites of interest would be advantageous for improving the capabilities of MRI. An attractive method to accomplish this is to tailor particle size within a range for which relaxivity is maximized, known as the static dephasing regime (SDR).[6] However, SPIONs with diameters approaching such an optimal size often become permanently magnetic,[7] resulting in uncontrolled aggregation that diminishes relaxivity and substantially reduces the SPION's ability to reach target sites. Assembling SPIONs in the form of clusters has emerged as a promising strategy to yield a desired size of metallic core while maintaining superparamagnetism and colloidal stability.[8–14] A limitation of common approaches, however, lies in the SPION coating material used to induce clustering, as such materials may limit penetration of water near the metallic core or reduce hydrophilic interactions. Such factors are intrinsically detrimental since the effectiveness of an MR contrast agent is highly dependent on its ability to interact with surrounding water.[15]

In this study, we hypothesized that the globular nature of a hydrophilic, hyperbranched polymer would allow for maximal MR relaxivity of clustered SPIONs to improve the diagnostic capability of *in vivo* imaging of ischemic tissue. To test this hypothesis, SPIONs were coated by a hyperbranched polyglycerol substituted with a varying number of octadecyl chains (HPG-g-C_{18}) to form the nanoclusters (Figure 1a). Hyperbranched polyglycerol was adopted to mimic the structure of glycogen, a natural, hyperbranched biopolymer that is able to hold 2–3 times its weight in water.[16] The critical role of the polyglycerol molecular architecture in enhancing relaxivity of SPION clusters was addressed using the analogous linear polyglycerol substituted with octadecyl chains as a control. The ability of the resultant ultrasensitive nanocluster to identify ischemic tissue vascularized with leaky blood vessels was then evaluated in a murine model of hindlimb ischemia.[17]

2. Materials and Methods

All materials were purchased from Sigma-Aldrich unless otherwise noted.

2.1 General polyglycerol characterization methods

Mass spectral analysis was performed using ESI on a Waters Micromass Q-Tof spectrometer or MALDI-TOF on an Applied Biosystems Voyager-DE STR spectrometer. Nuclear magnetic resonance (NMR) spectra were recorded on a Varian U400, UI400, U500 or VXR500 spectrometer. Additionally, the molecular weights of HPGs were evaluated by gel permeation chromatography (GPC, Waters Breeze 2) with a Styragel HT column. 20 mM LiBr in *N*,*N*-dimethylformamide (DMF) was used as an eluent. Values were based on calibration against polyethylene glycol (PEG) standards.

2.2 Synthesis of HPG

The overall synthetic scheme is shown in Figure S1 and generally follows the methods reported by Kong, Zimmerman, and coworkers.[18] To prepare HPG, sodium hydride (NaH) was mixed with the alkyne initiator, 4-pentyn-1-ol at a 1:10 molar ratio. The mixture was stirred for 15 min followed by addition of doubly distilled glycidol by a syringe pump (1.2 mL/h) while stirring at 70 °C. The molar ratio of glycidol to initiator was varied to achieve different molecular weights. After addition, the reaction continued for 3 h with constant stirring. For each 1 mL of glycidol used, 2 mL of methanol was added and ion exchange Amberlite IR 1200 H form prewashed resin was added to the polymer solution and stirred for 1 h at 50 °C. The resin was removed by vacuum filtration and the polymer was fractionally precipitated with cold ether and centrifuged at 4,000 rpm for 15 min at 4 °C. The supernatant was decanted and precipitation was repeated 2–3 more times. The resulting HPGs were characterized by mass spectrometry, ^{1}H NMR, and ^{13}C NMR.

2.3 Alkylation of HPG

HPG (40 mg, 0.005 mmol) was dissolved in anhydrous dimethylformamide (DMF, 2.5 mL) to which NaH in 60% mineral oil (7.6 mg, 0.19 mmol) was added. The solution was stirred for 15 min before addition of bromooctadecane (63.3 mg, 0.19 mmol). The average number of conjugated alkyl chains was controlled by varying the ratio of bromooctadecane to HPG. The reaction mixture was then placed in a preheated oil bath at 80 °C for 24 h. The mixture was extracted with hexane 3 times to remove unreacted bromide and the DMF was removed first by rotary evaporator and then by high vacuum. The material was characterized by MALDI-TOF, ^{1}H NMR and ^{13}C NMR.

The degree of substitution of alkyl chain (DS_{C18}) on alkylated HPG was calculated from the integrated peaks of the ^{1}H NMR spectra as follows in Eq. (1):

$$DS_{C18} = \frac{(Peak_{1.3}/30)}{(Peak_{4.0-3.4}/5) - (Peak_{1.3}/30)} \times 100\% \quad (1)$$

2.4 FITC-labeling of alkylated HPG

Fluorescently-labeled HPG was used for analysis of nanocluster transport in the transwell assay described in 2.14. To modify HPG for this experiment, alkylated HPG was dissolved in anhydrous DMF. NaH (0.17 mmol) was then added and stirred at room temperature for 5–15 minutes. Fluorescein isothiocyanate (FITC, 0.17 mmol) was added to the flask and protected from light, and the mixture stirred for 24 h at room temperature. The material was purified by dissolving it in methanol, followed by precipitation in cold diethyl ether, and finally, dialysis in a 1000 MWCO membrane against a water/10% methanol/$NaHCO_3$ saturated solution and brine.

2.4 Synthesis of the LPG intermediate, ethyl glycidol ether (EEGE) (3 in Figure S1b)

Freshly distilled glycidol was added to ethyl vinyl ether at a molar ratio of 0.8:3 and cooled to 0 °C. p-Toluene sulfonic acid monohydrate (pTSA) was added slowly while keeping the temperature below 20 °C. The mixture was then warmed to room temperature and stirred for

3 h. Saturated $NaHCO_3$ was added and the organic layer was dried over Na_2SO_4. Solvent was removed under vacuum and the product was stored with CaH and vacuum distilled at 50 °C. The product was characterized by ^1H NMR, ^{13}C NMR, and electrospray ionization (ESI) mass spectrometry on a Waters Micromass Q-Tof spectrometer.

2.5 Synthesis of the LPG intermediate, poly(EEGE) (5 in Figure S1b)

Using a slightly modified literature procedure,[19, 20] 2.1 mmol of 4-pentyn-1-ol (0.2 mL) was added to 15 mL freshly distilled diglyme, followed by 0.2 mL of a 1 M solution of potassium tert-butoxide in THF and stirred for 10 min. The flask was then cooled to −50 °C prior to dropwise addition of EEGE (92 mL, 725 mmol). The reaction continued for 48 h at 120 °C. Diglyme was removed by vacuum distillation at 80 °C, and the remaining product was dissolved in dichloromethane (DCM) and washed with water. The organic phase was dried over anhydrous sodium carbonate, and the solvent was removed using a rotary evaporator. The product was characterized by MALDI-TOF, ^1H NMR, and ^{13}C NMR.

2.6 Synthesis and alkylation of LPG

First, poly(EEGE) was dissolved in THF, followed by addition of 32% HCl aqueous solution, which resulted in precipitation of LPG. The reaction continued for 2 h before the solvent was decanted and the residue was washed twice with THF, followed by solvent removal under vacuum. Next, as in the alkylation of HPG, LPG was dissolved in anhydrous DMF and reacted with bromooctadecane in the presence of NaH to yield LGP_{3k}-g-C_{18}(2). The products were characterized by MALDI-TOF, ^1H NMR and ^{13}C NMR. DS_{C18} was determined with Eq. (1), as in the case of alkylated HPG.

2.7 Contact angle measurement of HPG and LPG

HPG_{3k} or LPG_{3k} was dissolved in a 1:1 water and acetone mixture and spin coated on glass cover slides to make a thin, even film using a VTC-100 vacuum spin coater (MTI Corporation). A droplet of deionized water was placed on the film, and the contact angle was measured by a contact angle goniometer (Rame-Hart). The surface energies of the polyglycerol films, *W*, were calculated from the contact angle, θ, using the Young-Dupre equation and the surface tension of water, γ:

$$W=\gamma(1+\cos\theta) \quad (2)$$

2.8 Synthesis of oleic acid-capped SPIONs

5 nm-diameter oleic acid-capped SPIONs were synthesized by thermal decomposition of iron acetylacetonate, as previously described.[21, 22] Briefly, iron acetylacetonate (2 g), oleylamine (660 μL), oleic acid (660 μL), and 1,2 dodecanediol (0.7 g) were dissolved in 6.7 mL of benzyl ether. The mixture was heated under nitrogen to 200 °C for 2 h, followed by reflux at 300 °C for 1 h. SPIONs were purified by precipitation in ethanol, magnetic separation, and finally redispersion in chloroform at a concentration of 10 mg/mL.

2.9 Analysis of magnetization of SPIONs

The field-dependent magnetization of the SPIONs was evaluated with a vibrating sample magnetometer (MPMS, Quantum Design). Iron concentration was determined by digestion of SPIONs in concentrated nitric acid followed by analysis with inductively coupled plasma optical emission spectroscopy (ICP-OES, Perkin-Elmer Optima 2000 DV). The saturation magnetization acquired with the MPMS was used to estimate the theoretical maximum relaxivity within the static dephasing regime (SDR) using Eq. (3):

$$r_2 = \frac{2\pi\gamma\mu_0\nu M_s}{9\sqrt{3}} \quad (3)$$

where γ is here defined as the proton gyromagnetic ratio, μ_0 is the permeability of free space, υ is the molar volume, and M_s is the saturation magnetization. With a saturation magnetization of 71 emu/g, the maximum relaxivity for such SPIONs yielded the value of 742 $mM^{-1}s^{-1}$.

2.10 Fabrication of polyglycerol-coated SPION nanoclusters

SPION clusters were fabricated by emulsification. The aqueous phase was prepared by dissolving HPG-g-C_{18} or LPG-g-C_{18} in deionized water at varying concentrations. SPIONs dispersed in chloroform were added to the PG aqueous solution, and the mixtures were immediately sonicated (Fisher Scientific Sonic Dismembrator, Model 100). Chloroform was then removed by rotary evaporation (Heidolph Hei-VAP), and any excess material was removed by centrifugation. For the transwell assay described in section 2.14, the FITC-labeled HPG-g-C_{18} was used to induce SPION clustering.

2.11 Size determination of nanoclusters

The Z-average hydrodynamic diameters of the nanoclusters were determined by dynamic light scattering (DLS, Malvern Zetasizer Nano ZS). TEM micrographs were obtained by JEOL 2100 cryo TEM at 200 kV, with samples dried on holey carbon-coated copper grids. To demonstrate stability in serum, HPG-SPIONs were incubated for 2 h at 37 °C in phosphate buffered saline (PBS) supplemented with 50% type AB human serum off the clot (PAA Laboratories Inc.) prior to grid preparation. For certain experiments, the cryo-TEM sample was applied to a lacey carbon-coated copper grid and prepared by cryo plunge (FEI vitrobot) into liquid ethane (~90 K) in a controlled environment at 23 °C and 100% humidity. The images were acquired using JEOL 2100 cryo TEM with a cryogenic sample holder (Gatan 626) at 60 kV with digital imaging. Cluster core size was determined from a minimum of 50 clusters using ImageJ software.

2.12 T_2 relaxivity measurement of SPION contrast agents

MR phantoms of SPIONs were prepared in borosilicate culture tubes, which were immobilized in an agar gel. Imaging was performed with a 3 T Siemens Magnetom Trio scanner equipped with head coil. Images were acquired using a spin echo sequence with repetition time (TR) of 1200 ms and echo time (TE) varied from 12 to 490 ms to determine spin-spin relaxation time (T_2) by nonlinear least-squares curve fitting to Eq. (4):

$$S(\mathrm{TE}) = S_0 e^{-\mathrm{TE}/T_2} + b \quad (4)$$

where S(TE) is the average signal intensity for echo time (*TE*) taken over the coronal section area of the MR phantom by ImageJ software, S_0 represents the steady state signal intensity, and b is an offset due to the background noise level. Transverse molar relaxivity (r_2) was then determined by linear regression of Eq. (5):

$$1/T_2 = 1/T_{2,\mathrm{water}} + r_2[\mathrm{Fe}] \quad (5)$$

in which $1/T_{2,\mathrm{water}}$ is the relaxation rate of water and [Fe] is the iron concentration within the phantom sample. Iron concentration was determined by ICP-OES (Perkin-Elmer Optima 2000 DV) after digestion in concentrated nitric acid. Performance of HPG-SPIONs was compared to the unclustered SPION, FeREX (BioPAL, Inc.), with a 5 nm diameter core. FeREX is a preparation similar to the commercial product, Feridex, which has a T_2 relaxivity of 120 $mM^{-1}s^{-1}$.[23]

2.13 MTT assay for cellular metabolic activity

C166 endothelial cells were seeded at a density of 5×10^3 cells per well in a 96-well plate. Cells were incubated for 24 h with SPION clusters coated with HPG_{50k}-g-C_{18}(2). MTT reagent ((3-(4,5-dimethylthiazol-2-yl)-2,5-diphenyltetrazolium bromide, ATCC) was then added, followed by addition of MTT detergent, and absorbance at 570 nm was measured with a plate reader (Tecan Infinite 200 PRO) as an indicator of metabolic activity.

2.14 Transwell migration assay

The setup consisted of an HTS Transwell 96-well plate with 8 μm diameter pores in a polyester membrane (Corning). C166 endothelial cells were seeded on the transwell insert at a density of 1×10^5 cells per well to form an endothelial layer according to the manufacturer's protocol. To compare physiological to inflamed states, cells were incubated overnight with a 10 ng/mL solution of tumor necrosis factor alpha (TNF-α, GenScript Corporation) to induce an inflammatory condition. Cells were then incubated for 1 h with FITC-labeled HPG-SPIONs, and fluorescence intensity of the receiver well was measured with a plate reader (Tecan Infinite 200 PRO) at excitation of 458 nm and emission at 535 nm as an indication of the clusters' ability to permeate the endothelial layer.

2.15 Hindlimb ischemia model

Hindlimb ischemia was induced in male BALB/c mice (Jackson Laboratories, ME) in accordance with the protocol approved by the Illinois Institutional Animal Care and Use Committee. Mice were anesthetized by intraperitoneal injection of a mixture of xylazine (10 mg/kg) and ketamine hydrochloride (100 mg/kg). A small incision was made on the upper thigh of the left hindlimb and the femoral artery was ligated in two regions with 5-0 Ethilon sutures (Johnson and Johnson, NJ). The artery was then severed between the proximal and distal sutures. The ischemic injury developed over 24 h, at which point HPG-SPIONs or FeREX were injected *via* tail vein at a dose of 2 mg Fe/kg. 2 mice were evaluated per condition.

2.16 In vivo MRI

Mice were imaged 3 h after contrast agent injection and compared to a mouse that received the ischemic injury but no contrast agent. Imaging was performed with a Varian 14.1 T microimager consisting of a Unity/Inova 600 MHz NMR spectrometer and adjustable radiofrequency coil. Coronal images were acquired using a spin-echo multislice (SEMS) pulse sequence with TR = 500 ms, TE = 20 ms, and slice thickness = 0.5 mm.

The contrast-to-noise ratio (CNR) was calculated from Eq. (6):

$$CNR = \frac{|S_{ROI} - S_{muscle}|}{\sigma_{noise}} \quad (6)$$

where *S* is the grayscale signal intensity value of the region of interest (ROI) or surrounding muscle, and σ is standard deviation.

2.17 Histological analysis

The mouse thigh was split into 4 sections between hip and knee, fixed in 10% buffered formalin, and embedded in paraffin. Tissues were cut at a 4 μm thickness using a Leica RM 2255 rotary microtome and the cross-sections were stained with Hematoxylin and Eosin or Prussian blue stain to analyze tissue morphology and locate SPIONs, respectively. Tissue sections were visualized with a NanoZoomer Slider Scanner/Digital Pathology System (Hamamatsu).

3. Results and Discussion

3.1 Synthesis and characterization of polyglycerol-coated SPION nanoclusters

First, hyperbranched polyglycerol (HPG) was synthesized by one-step anionic ringopening polymerization of glycidol (Figure S1a). Further reaction of HPG with octadecyl bromide yielded HPG with a molecular weight of 3 kg/mol substituted with an average of 5 alkyl chains per polymer, termed HPG_{3k}-g-C_{18}(5), according to NMR and mass spectrometry (Figures 1a and S2–S3). The control, linear polyglycerol (LPG) with a molecular weight of 3 kg/mol was synthesized through a three-step process in which glycidol was reacted with ethyl vinyl ether to form ethoxy ethyl glycidyl ether, which was then polymerized and finally hydrolyzed to yield LPG (Figure S1b). Subsequent alkylation of the resultant LPG_{3k} yielded LPG_{3k}-g-C_{18}(2), with an average of 2 octadecyl chains per polymer (Figures 1a and S4–S7). Despite having similar molecular weights and chemical functionalities, the hyperbranched architecture of HPG resulted in a smaller contact angle than the LPG (Figure S8). The corresponding surface energy of the HPG film was more than 30% greater. The result indicates that coating of SPION clusters with HPG would be advantageous in facilitating interaction with surrounding water.

Emulsification of 5 nm-diameter oleic acid-capped SPIONs initially dispersed in chloroform and polyglycerol dissolved in water resulted in spherical SPION clusters that were stable in water (Figures 1b and 1c), as confirmed with transmission electron microscopy (TEM) (Figure 1d). While the *Z*-average hydrodynamic diameter determined by dynamic light scattering (DLS) was 80 nm regardless of polyglycerol molecular architecture, the average

core size of the HPG_{3k}-g-C_{18}(5) clusters measured with TEM was 42±9 nm, and that of the LPG_{3k}-C_{18}(2)-induced clusters was 60±13 nm. This indicates that HPG_{3k}-g-C_{18}(5) provides a thicker hydrated polymer coating layer. In both cases, SPION clusters remained dispersed for over one year. Relaxivity measurements were performed on the nanoclusters to determine effects of the hyperbranched structure on T_2 relaxation (Figure 1e). Despite having the same hydrodynamic size, nanoclusters coated by HPG_{3k}-g-C_{18}(5) had a relaxivity 30% higher than clusters made with LPG_{3k}-g-C_{18}(2), due to differences in hydrophilicity and coating thickness as a result of the globular, branched structure.

3.2 Tuning cluster size for relaxivity enhancement

Next, the size of the nanoclusters was tuned within the SDR, commonly centered on a diameter of 120 nm.[24] Size has been shown to vary with polymer content during fabrication,[25–28] however, clusters made with HPG_{3k}-g-C_{18}(5) or LPG_{3k}-g-C_{18}(2) remained 80 nm, regardless of concentration (Figure S9), with core diameters of approximately 40 nm and 60 nm respectively. To strengthen potential HPG-mediated inter-droplet interactions,[29] a larger HPG with a molecular weight of 50 kg/mol, termed HPG_{50k}, was synthesized by increasing the ratio of glycidol-to-initiator in the polymerization reaction (Figure S1a).

The resulting HPG was alkylated at two levels to yield HPG_{50k}-g-C_{18}(2) and HPG_{50k}-g-C_{18}(10), in which two and ten alkyl chains were conjugated to the HPG_{50k} respectively (Figures S10–S13). For these polymers, the hydrodynamic diameter of the nanoclusters was indeed tunable with HPG content (Figure 2a), with average diameters increasing to a critical size of approximately 145 nm. In most cases, the system was well controlled, with a polydispersity index (PDI) below 0.2 (Figure S14). However, for the larger clusters approaching a 140 nm diameter, the PDI was between 0.2–0.3, indicating a wider size distribution in such samples. TEM images of SPION clusters also verified that the diameter of the clustered metallic core was tailored with HPG_{50k}-g-C_{18}, following the same trends as the hydrodynamic diameter measured with DLS (Figure 2b).

MR relaxivity of nanoclusters coated by alkylated HPG_{50k} displayed the size-dependent behavior, characterized by an initial increase in relaxivity followed by decrease with larger sizes (Figure 3a). Additionally, for any given size, the more highly alkylated HPG (i.e., HPG_{50k}-g-C_{18} (10)) led to reduced relaxivity (Figure 3a(i)), which is likely due to differences in hydrophilicity as a result of the alkylation. As such, tuning the diameter of SPION nanoclusters coated with HPG_{50k}-g-C_{18}(2) led to a relaxivity of 719 $mM^{-1}s^{-1}$ (Figure 3a(ii)). This relaxivity was close to the theoretical maximum for the SPIONs used, which was determined to be 742 $mM^{-1}s^{-1}$ based on magnetic saturation (Figure S15). The low PDI may also have assisted in the tuning of clusters within the appropriate size regime for relaxivity optimization. On the contrary, the larger clusters with diameters above 135 nm had high PDIs, which may have further contributed to their reduced relaxivities.

According to phantom images, the HPG-SPIONs with a relaxivity of 719 $mM^{-1}s^{-1}$ provided high contrast against background at low iron levels, unlike unclustered SPIONs with measured relaxivity of 122 $mM^{-1}s^{-1}$ (Figure 3b). The nanoclusters completely dephased the water proton signal at an iron concentration of 0.14 mM, whereas unclustered SPIONs at the same concentration provided no noticeable contrast. Clinically-used formulations of iron

oxide nanoparticles, such as Feridex, Sinerem, and ferumoxytol, would be expected to perform similarly to the unclustered SPIONs shown, as they have reported T_2 relaxivities of 120, 65, and 89 $mM^{-1}s^{-1}$ respectively.[23]

3.3 In vitro characterization and in vivo evaluation of nanoclusters

The SPION nanoclusters minimally influenced metabolic activity of C166 endothelial cells, even at high doses of 580 μg Fe/mL (Figure S16). Furthermore, the ability of the clusters to penetrate an inflamed endothelium as a method of passive targeting was simulated using a transwell system (Figure S17). The migration of clusters through an endothelial monolayer was greatly enhanced after incubating the cells with tumor necrosis factor (TNF)-α, a proinflammatory cytokine.[30] SPION nanoclusters also remained intact during incubation in serum, thus supporting their stable structural integrity in blood circulation (Figure S18).

Finally, the engineered HPG-SPIONs were used to evaluate their capacity to accumulate in and identify ischemic tissue *in vivo* following systemic injection. Ligation of the femoral artery resulted in inflammation and local tissue damage typical of ischemic wounds (Figure S19a). HPG-SPIONs injected systemically *via* tail vein were able to dramatically reduce MR signal in the injured region of the thigh at a dose of 2 mg Fe/kg, which is 5 to 10 fold lower than those used in similar studies[31–33] (Figure 4). In contrast, the unclustered SPIONs provided minimal enhancement and a correspondingly lower contrast-to-noise ratio (CNR). This was despite having a comparable amount of iron accumulated in the target tissue as verified with Prussian blue staining (Figure S19b).

In summary, this study demonstrates that HPG creates SPION clusters with very high relaxivity due to control of cluster size coupled with optimization of hydrophilicity at the surface. We propose that the thick, hydrophilic HPG coating layer serves to enhance relaxivity by absorbing water and reducing its diffusivity,[34] analogous to the way the multi-branched polysaccharide, glycogen, interacts with and retains water *via* its molecular architecture and extensive hydrogen bonding. While others have examined the effects of SPION composition, or of clustering to attain a desired aggregate size, this study has focused on the effects of the coating material of the cluster to further optimize relaxivity. Specifically, this study distinguishes itself as a first time investigation into the effects of molecular architecture of the packaging material on performance of the SPIONs. Such hydrophilic coatings may also be applied to improving nanoparticles of varying size and composition, and is thus broadly applicable in contrast agent design.

4. Conclusions

The formulated HPG-SPION nanoclusters can identify tissue defects using MRI, and therefore have potential to diagnose a wide variety of vascular diseases, which remain a leading cause of death worldwide. For further improvement, the HPG could easily be modified with targeting moieties to actively bind nanoclusters to sites of interest. Furthermore, as the inflammation that induces leaky vasculature occurs during initial stages of diseases, the HPG-coated SPION clusters may represent an early detection system for some of the most significant diseases, not only for vascular diseases, but also cancer.

Supplementary Material

Refer to Web version on PubMed Central for supplementary material.

Acknowledgment

The authors thank B. Odintsov and R. Larsen at the Beckman Institute for Advanced Science and Technology for help with MRI, as well as J. Atkinson and D. Van Harlingen for magnetometry measurements at the University of Illinois at Urbana-Champaign. Mass spectral analyses were provided by the Mass Spectrometry Laboratory, School of Chemical Sciences, and TEM and DLS were carried out in the Frederick Seitz Materials Research Laboratory Central Facilities at the University of Illinois. Work was funded by the National Institutes of Health (1R01 HL109192 to H.J.K., S.C.Z., and S.M., 1R01 HL098967 to S.M., Chemistry-Biology Interface Training Grant 5T32-GM070421 to C.E.S.) and The Center for Advanced Study at the University of Illinois.

References

1. Cheon J, Lee J-H. Synergistically Integrated Nanoparticles as Multimodal Probes for Nanobiotechnology. Acc. Chem. Res. 2008; 41:1630–1640. [PubMed: 18698851]
2. Lee N, Hyeon T. Designed Synthesis of Uniformly Sized Iron Oxide Nanoparticles for Efficient Magnetic Resonance Imaging Contrast Agents. Chem. Soc. Rev. 2012; 41:2575–2589. [PubMed: 22138852]
3. Tsushima S, Teranishi K, Hirai S. Magnetic Resonance Imaging of the Water Distribution within a Polymer Electrolyte Membrane in Fuel Cells. Electrochem. Solid-State Lett. 2004; 7:A269–A272.
4. Elkins CJ, Markl M, Pelc N, Eaton JK. 4D Magnetic Resonance Velocimetry for Mean Velocity Measurements in Complex Turbulent Flows. Exp. Fluids. 2003; 34:494–503.
5. Cha C, Kim SY, Cao L, Kong H. Decoupled Control of Stiffness and Permeability with a Cell-Encapsulating Poly(Ethylene Glycol) Dimethacrylate Hydrogel. Biomaterials. 2010; 31:4864–4871. [PubMed: 20347136]
6. Yablonskiy DA, Haacke EM. Theory of NMR Signal Behavior in Magnetically Inhomogeneous Tissues: The Static Dephasing Regime. Magn. Reson. Med. 1994; 32:749–763. [PubMed: 7869897]
7. Lee N, Kim H, Choi SH, Park M, Kim D, Kim H-C, Choi Y, Lin S, Kim BH, Jung HS, et al. Magnetosome-Like Ferrimagnetic Iron Oxide Nanocubes for Highly Sensitive MRI of Single Cells and Transplanted Pancreatic Islets. Proc. Natl. Acad. Sci. 2011; 108:2662–2667. [PubMed: 21282616]
8. Pöselt E, Kloust H, Tromsdorf U, Janschel M, Hahn C, Maßlo C, Weller H. Relaxivity Optimization of a PEGylated Iron-Oxide-Based Negative Magnetic Resonance Contrast Agent for T_2-Weighted Spin-Echo Imaging. ACS Nano. 2012; 6:1619–1624. [PubMed: 22276942]
9. Lee HJ, Jang K-S, Jang S, Kim JW, Yang H-M, Jeong YY, Kim J-D. Poly(Amino Acid)S Micelle-Mediated Assembly of Magnetite Nanoparticles for Ultra-Sensitive Long-Term MR Imaging of Tumors. Chem. Commun. 2010; 46:3559–3561.
10. Ai H, Flask C, Weinberg B, Shuai XT, Pagel MD, Farrell D, Duerk J, Gao J. Magnetite-Loaded Polymeric Micelles as Ultrasensitive Magnetic-Resonance Probes. Adv. Mater. 2005; 17:1949–1952.
11. Taboada E, Solanas R, Rodríguez E, Weissleder R, Roig A. Supercritical-Fluid-Assisted One-Pot Synthesis of Biocompatible Core(γ-Fe_2O_3)/Shell(SiO_2) Nanoparticles as High Relaxivity T2-Contrast Agents for Magnetic Resonance Imaging. Adv. Funct. Mater. 2009; 19:2319–2324.
12. Tan H, Xue JM, Shuter B, Li X, Wang J. Synthesis of PEOlated Fe_3O_4@SiO_2 Nanoparticles via Bioinspired Silification for Magnetic Resonance Imaging. Adv. Funct. Mater. 2010; 20:722–731.
13. Paquet C, de Haan HW, Leek DM, Lin H-Y, Xiang B, Tian G, Kell A, Simard B. Clusters of Superparamagnetic Iron Oxide Nanoparticles Encapsulated in a Hydrogel: A Particle Architecture Generating a Synergistic Enhancement of the T_2 Relaxation. ACS Nano. 2011; 5:3104–3112. [PubMed: 21428441]
14. Yoon T-J, Lee H, Shao H, Hilderbrand SA, Weissleder R. Multicore Assemblies Potentiate Magnetic Properties of Biomagnetic Nanoparticles. Adv. Mater. 2011; 23:4793–4797. [PubMed: 21953810]

15. Smith CE, Shkumatov A, Withers SG, Yang B, Glockner JF, Misra S, Roy EJ, Wong C-H, Zimmerman SC, Kong H. A Polymeric Fastener Can Easily Functionalize Liposome Surfaces with Gadolinium for Enhanced Magnetic Resonance Imaging. ACS Nano. 2013; 7:9599–9610. [PubMed: 24083377]
16. Geddes, R. Glycogen: A Structural Viewpoint. In: Aspinal, GO., editor. The Polysaccharides. Vol. 3. New York: Academic Press; 1985. p. 283-336.
17. Limbourg A, Korff T, Napp LC, Schaper W, Drexler H, Limbourg FP. Evaluation of Postnatal Arteriogenesis and Angiogenesis in a Mouse Model of Hind-Limb Ischemia. Nat. Protocols. 2009; 4:1737–1748. [PubMed: 19893509]
18. Zill A, Rutz AL, Kohman RE, Alkilany AM, Murphy CJ, Kong H, Zimmerman SC. Clickable Polyglycerol Hyperbranched Polymers and Their Application to Gold Nanoparticles and Acid-Labile Nanocarriers. Chem. Commun. 2011; 47:1279–1281.
19. Kainthan RK, Janzen J, Levin E, Devine DV, Brooks DE. Biocompatibility Testing of Branched and Linear Polyglycidol. Biomacromolecules. 2006; 7:703–709. [PubMed: 16529404]
20. Stiriba S-E, Kautz H, Frey H. Hyperbranched Molecular Nanocapsules: Comparison of the Hyperbranched Architecture with the Perfect Linear Analogue. J. Am. Chem. Soc. 2002; 124:9698–9699. [PubMed: 12175215]
21. Clay N, Baek K, Shkumatov A, Lai M-H, Smith CE, Rich M, Kong H. Flow-Mediated Stem Cell Labeling with Superparamagnetic Iron Oxide Nanoparticle Clusters. ACS Appl. Mater. Interfaces. 2013; 5:10266–10273. [PubMed: 24033276]
22. Sun S, Zeng H, Robinson DB, Raoux S, Rice PM, Wang SX, Li G. Monodisperse MFe_2O_4 (M = Fe, Co, Mn) Nanoparticles. J. Am. Chem. Soc. 2003; 126:273–279. [PubMed: 14709092]
23. Laurent S, Forge D, Port M, Roch A, Robic C, Vander Elst L, Muller RN. Magnetic Iron Oxide Nanoparticles: Synthesis, Stabilization, Vectorization, Physicochemical Characterizations, and Biological Applications. Chem. Rev. 2008; 108:2064–2110. [PubMed: 18543879]
24. Vuong QL, Berret J-F, Fresnais J, Gossuin Y, Sandre O. A Universal Scaling Law to Predict the Efficiency of Magnetic Nanoparticles as MRI T2-Contrast Agents. Adv. Healthc. Mater. 2012; 1:502–512. [PubMed: 23184784]
25. Dey P, Blakey I, Thurecht KJ, Fredericks PM. Self-Assembled Hyperbranched Polymer-Gold Nanoparticle Hybrids: Understanding the Effect of Polymer Coverage on Assembly Size and SERS Performance. Langmuir. 2012; 29:525–533. [PubMed: 23244573]
26. Pöselt E, Fischer S, Foerster S, Weller H. Highly Stable Biocompatible Inorganic Nanoparticles by Self-Assembly of Triblock-Copolymer Ligands. Langmuir. 2009; 25:13906–13913. [PubMed: 19663518]
27. Murthy AK, Stover RJ, Borwankar AU, Nie GD, Gourisankar S, Truskett TM, Sokolov KV, Johnston KP. Equilibrium Gold Nanoclusters Quenched with Biodegradable Polymers. ACS Nano. 2012; 7:239–251. [PubMed: 23230905]
28. Paquet C, Pagé L, Kell A, Simard B. Nanobeads Highly Loaded with Superparamagnetic Nanoparticles Prepared by Emulsification and Seeded-Emulsion Polymerization. Langmuir. 2009; 26:5388–5396. [PubMed: 20000392]
29. Israelachvili, JN. Steric (Polymer-Mediated) and Thermal Fluctuation Forces. In: Israelachvili, JN., editor. Intermolecular and Surface Forces. San Diego: Academic Press; 2011. p. 381-413.
30. Burke-Gaffney A, Keenan AK. Modulation of Human Endothelial Cell Permeability by Combinations of the Cytokines Interleukin-1 Alpha/Beta, Tumor Necrosis Factor-Alpha and Interferon-Gamma. Immunopharmacology. 1993; 25:1–9. [PubMed: 8320078]
31. Lee JH, Huh YM, Jun YW, Seo JW, Jang JT, Song HT, Kim S, Cho EJ, Yoon HG, Suh JS, et al. Artificially Engineered Magnetic Nanoparticles for Ultra-Sensitive Molecular Imaging. Nat. Med. 2007; 13:95–99. [PubMed: 17187073]
32. Lee N, Choi Y, Lee Y, Park M, Moon WK, Choi SH, Hyeon T. Water-Dispersible Ferrimagnetic Iron Oxide Nanocubes with Extremely High R_2 Relaxivity for Highly Sensitive in Vivo MRI of Tumors. Nano Lett. 2012; 12:3127–3131. [PubMed: 22575047]
33. Serkova NJ, Renner B, Larsen BA, Stoldt CR, Hasebroock KM, Bradshaw-Pierce EL, Holers VM, Thurman JM. Renal Inflammation: Targeted Iron Oxide Nanoparticles for Molecular MR Imaging in Mice. Radiology. 2010; 255:517–526. [PubMed: 20332377]

34. LaConte LE, Nitin N, Zurkiya O, Caruntu D, O'Connor CJ, Hu X, Bao G. Coating Thickness of Magnetic Iron Oxide Nanoparticles Affects R_2 Relaxivity. J. Magn. Reson. Imaging. 2007; 26:1634–1641. [PubMed: 17968941]

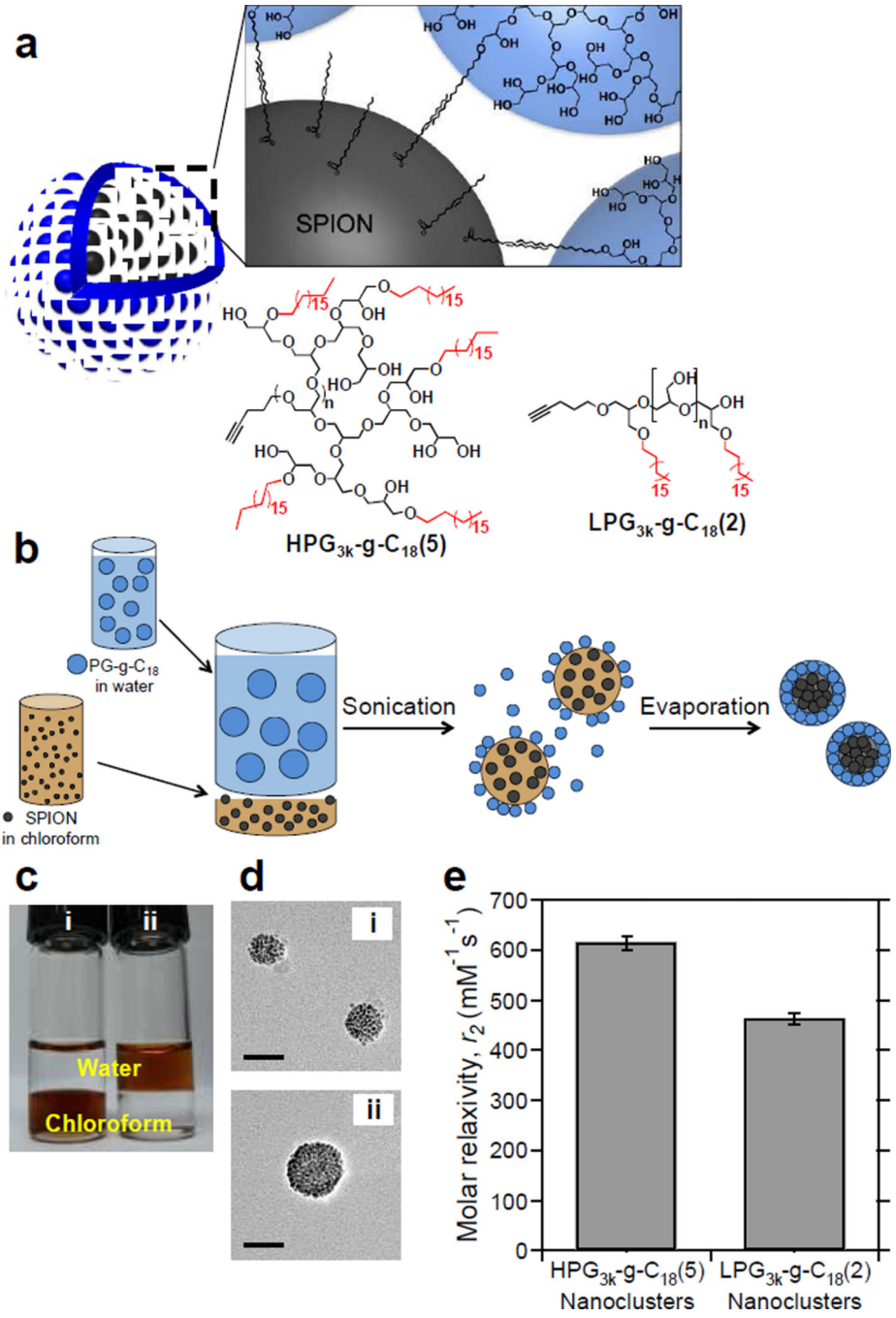

Figure 1.

HPG-coated SPION clusters. (a) Overall scheme of hyperbranched polyglycerolcoated SPION nanoclusters and representative chemical structures of HPG_{3k}-g-C_{18}(5) and LPG_{3k}-g-C_{18}(2). (b) Schematic of the emulsification process to create polyglycerol-coated SPIONs. (c) Oleic acid-capped SPIONs were dispersed in (i) chloroform before emulsification and in (ii) water after emulsification. (d) TEM micrographs of SPIONs coated with (i) HPG_{3k}-g-C_{18}(5) and (ii) LPG_{3k}-g-C_{18}(2). Scale bars represent 50 nm. A minimum of 50 clusters were

examined per condition. (e) Effect of molecular architecture on T_2 relaxivity. Error bars represent standard deviation of the fit parameter.

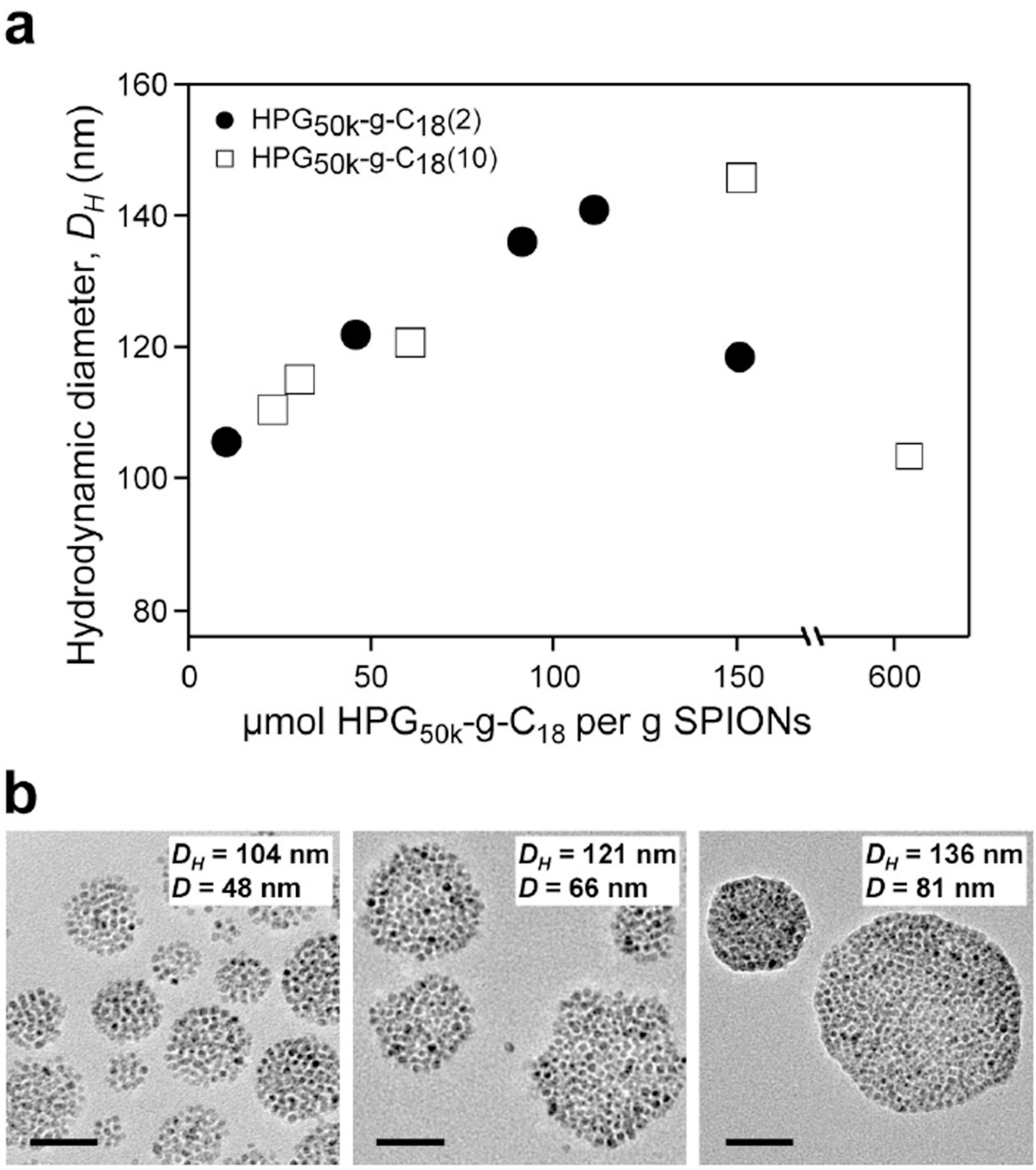

Figure 2.

Controlling size of SPION nanoclusters with high molecular weight HPG. (a) Control of Z-average hydrodynamic diameter (D_H) by varying the concentration of HPG_{50k}-g-C_{18}(2) (●) and HPG_{50k}-g-C_{18}(10) (□) per SPION, where HPG_{50k}-g-C_{18}(2) and HPG_{50k}-g-C_{18}(10) represent HPG_{50k} substituted with 2 and 10 C_{18} chains, respectively. Data are the average of three replicate measurements, with error bars representing standard deviation obscured by data point markers. (b) Representative TEM micrographs of SPION nanoclusters with

corresponding hydrodynamic diameter (D_H) determined from DLS and average core diameter (D) measured from a minimum of 50 clusters by TEM. Scale bars represent 50 nm.

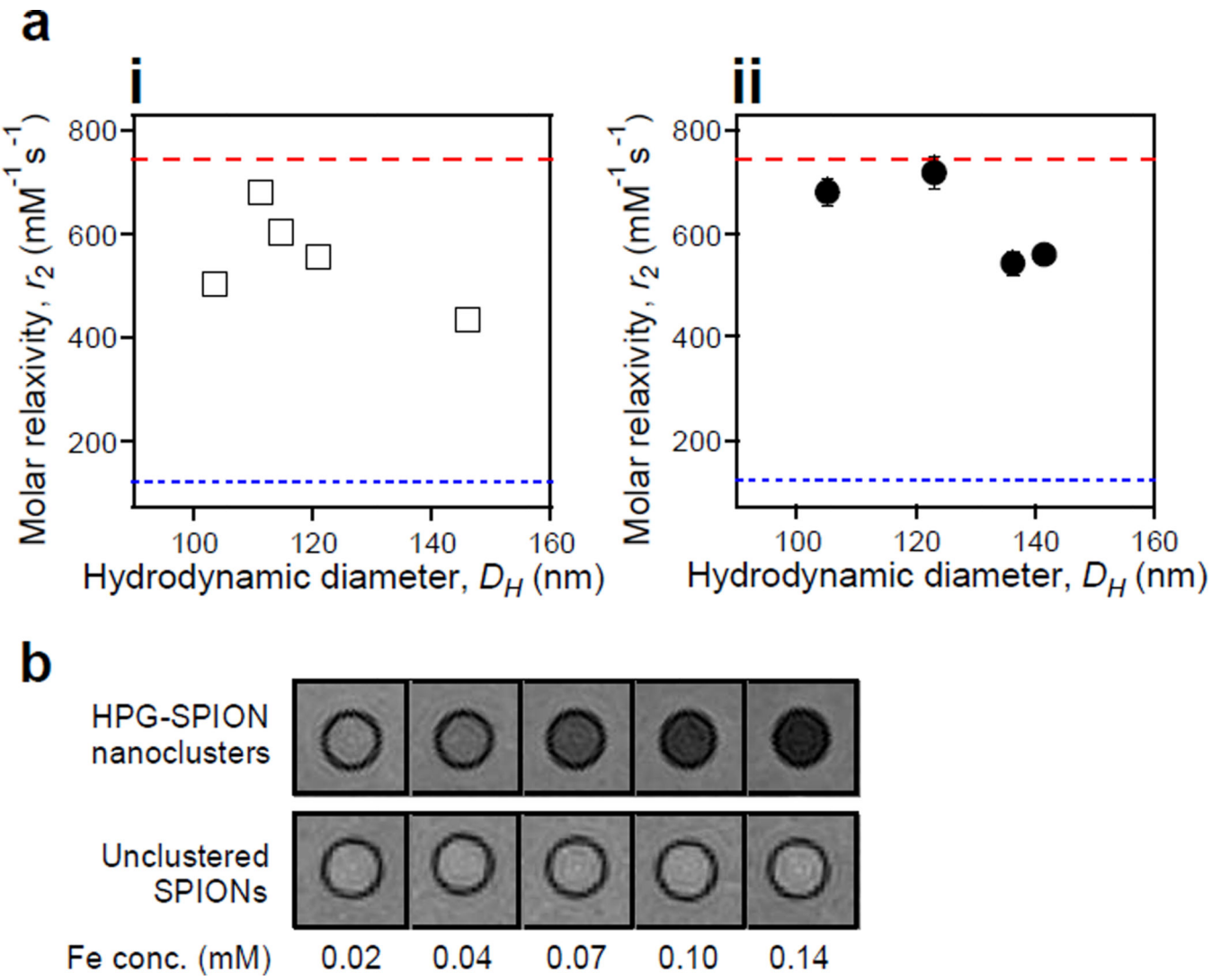

Figure 3.

Tuning relaxivity with cluster size. (a) Dependence of T_2 relaxivity (r_2) on the hydrodynamic diameter (D_H) of SPION clusters coated with (i) HPG_{50k}-g-C_{18}(10) and (ii) HPG_{50k}-g-C_{18}(2). The upper limit red dashed line represents the maximum theoretical relaxivity of the SPIONs at 742 $mM^{-1}s^{-1}$, while the lower blue dotted line at 122 $mM^{-1}s^{-1}$ is the relaxivity of unclustered, commercial SPIONs. All error bars represent standard deviation of the fit parameter and are partially obscured by data markers. (b) MR phantom images comparing nanoclusters with relaxivity of 719 $mM^{-1}s^{-1}$ to unclustered SPIONs with relaxivity of 122 $mM^{-1}s^{-1}$.

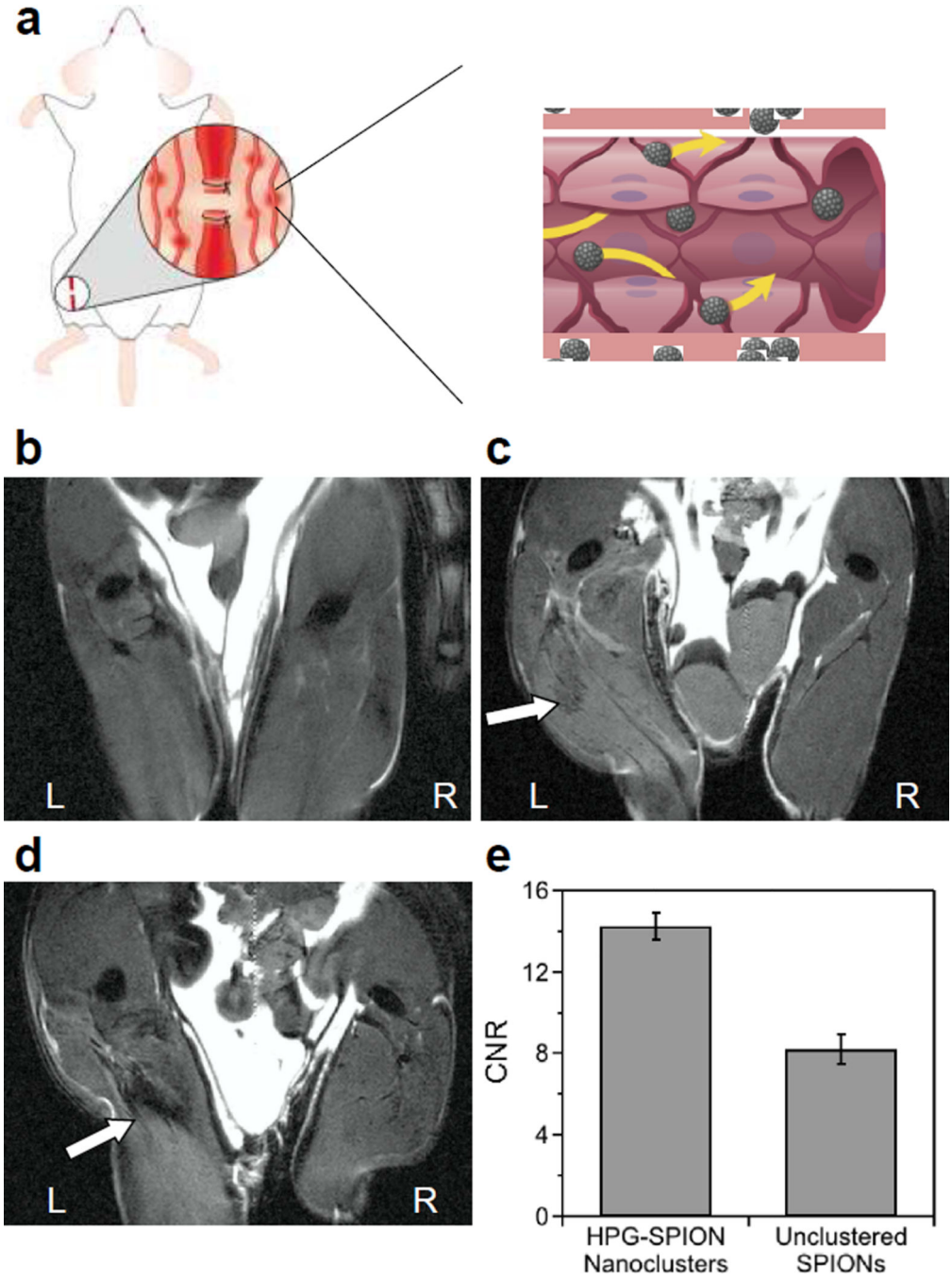

Figure 4.

In vivo evaluation of the ability of SPION nanoclusters to highlight damaged tissue in MR images. (a) Hindlimb ischemia was induced by ligation of the left femoral artery. A control mouse receiving no injection of contrast agent (b) is compared in coronal images to mice injected systemically with unclustered SPIONs (c) or the HPG-SPIONs with relaxivity of 719 $mM^{-1}s^{-1}$ (d). White arrows indicate negative contrast in the injured region of the thigh. (e) The contrast-to-noise ratio (CNR) in the region of interest compared to surrounding

muscle for HPG-SPION nanoclusters and unclustered SPIONs. Error bars are the standard deviation of 2 replicate mice per condition.